Computational Modeling of Current Density Distribution and Secondary Resistances for Aluminum Electrorefining in Ionic Liquids

M. K. Nahian, Y. Peng, L. Nastac, and R. G. Reddy

Abstract A numerical model was developed to simulate the current density distribution and secondary resistances for the aluminum electrorefining process from the room temperature ionic liquid (RTIL) consisting of 1-butyl-3-methylimidazolium chloride and aluminum chloride with the molar ratio of 2:1 ($AlCl_3$: BMIC). The materials and geometry were created based on the experimental parameters. The current density distribution was calculated via simulation. The effects of applied voltage, temperature, composition of the electrolyte, and the surface roughness of cathode on the secondary resistances were investigated in this research. It was found that the summation of contact and charge transfer resistance decreases with increasing the potential and the temperature as well as decreasing the surface roughness.

Keywords Process modeling and simulation · Ionic liquid · BMIC

Introduction

Industrial methods for producing aluminum require higher temperatures, which consume not only higher energy, but also are non-eco-friendly [1]. In recent years, room temperature ionic liquids (RTILs), which melt below 100 °C are showing a great promise to electrodeposit aluminum in a greenway at low temperatures. A mixture of imidazolium chloride-based ionic liquid such as 1-butyl-3-methylimidazolium chloride (BMIC) and aluminum chloride exhibit adherent, dendrite free deposition with high purity during aluminum electrorefining and electrowinning [2–4]. Several modelings have been developed to simulate the various type of cell conditions. Zhang and Reddy developed a mathematical 3-D model to forecast the current distribution, electric field distribution, fluid flow, and concentration for near room-temperature aluminum electrowinning cell using Ansys (paired with FLOTRAN and EMAG) and Ansys CFX programs [5, 6]. In this research, a model is developed to predict the

M. K. Nahian · Y. Peng · L. Nastac · R. G. Reddy (✉)
Department of Metallurgical and Materials Engineering, The University of Alabama, Tuscaloosa, AL 35487, USA
e-mail: rreddy@eng.ua.edu

TMS 2021 150th Annual Meeting & Exhibition Supplemental Proceedings,
The Minerals, Metals & Materials Series,
https://doi.org/10.1007/978-3-030-65261-6_89

current density distribution and secondary resistances for Al electrodeposition by using Ansys Fluent program. The electrolyte was an eutectic mixture of 1-butyl-3-methylimidazolium chloride (BMIC) and aluminum chloride ($AlCl_3$) in 1:2 (BMIC: $AlCl_3$) molar ratio where the anode is aluminum and the cathode is copper. Experimental data was used to calculate the contact resistance and investigate the electric potential distribution. This CFD software offers superior quality meshing, essential models for species transfer, electric potentials, fluid flow, heat transfer, solution accuracy, computational speed (allowing for parallel computations via domain decomposition), facilitating the implementation of complex boundary conditions and source terms via user-defined functions (UDF). This modeling study has five targets: 1. Analyzing the geometry and mesh of the model; 2. Analyzing the parameters on the boundary conditions; 3. Determining the properties of electrolyte and electrodes, such as density, viscosity, and electrical conductivity; 4. Calculating the contact resistance using experimental current density data; 5. Simulating the potential distribution on the electrodes and electrolyte.

Current density distribution plays an important role in the morphology of the deposition. Due to the geometry of the system, conductivity of cell component activation overpotential, diffusion overpotential and hydrodynamics of electrolyte, current density deviates in the different points of the electrode [7]. An accurate current density profile is possible to predict by using Ansys's Fluent modeling, which can help to estimate the electrodeposition morphology. If we consider the electrochemical cell as a simple electric circuit, we may define the current and potential in this way,

$$I = \frac{U}{R_s + R_e + R_c + R_{ct}}$$

where U is the electric potential, R_s is the resistance of solution, R_e is the resistance of the electrode, R_c is contact resistance between electrode and electrolyte, and R_{ct} is reaction resistance or charge-transfer resistance. Normally, solution resistance R_s and electrode resistance R_e contribute much more total resistance. So here, we consider contact resistance R_c and charge-transfer resistance R_{ct} as secondary resistances. Resistance at the interface between electrode and electrolytes plays an important role in the current density. Although the studies on this contact resistance have been done on energy storage systems, contact resistance studies on the electrodeposition method is rarely found [8–10]. When an electron transfers from the electrode to the electrolyte (or vice versa), it has to overcome the charge-transfer resistance. Conductivities of the solution were investigated in a previous study [11], and resistances of electrode materials were chosen from the modeling software. However, R_c and R_{ct} are necessary to be defined in the present work. Also, R_c is attributed to contacting interface of electrode and electrolyte, and R_{ct} is related to reaction, temperature, potential, as well as the concentration of reacted species. Therefore, the effect of temperature, potential, the concentration of Al species, type of ionic liquid, and surface morphology on secondary resistances are studied in the present work.

Process Modeling

The geometry of the electrochemical cell was developed by using the experimental cell dimensions. The diameter and height of the cylinder were 4 and 3 cm, respectively. The dimensions of the cathode electrode (Cu) were 1.5 × 1.5 × 0.1 cm, and the dimensions of the anode electrode (Al) were 1.5 × 1.5 × 0.15 cm. The distance between the two electrodes is 2.3 cm. One small cylinder with 0.5 cm height and 1 cm diameter was created at the bottom as a stirrer. All the above parameters are corresponding to the practical experiment. Then, a mesh with a good aspect ratio and skewness was established. The domain was filled with 1:2 mol ratio of BMIC-$AlCl_3$ as an ionic liquid electrolyte. Figure 1 shows the geometry and mesh of the model.

The quality of the geometry and mesh are listed in Table 1.

We selected the "Electrical potential" model. The steady-state and incompressible flow was assumed. And, the methods and equations used in this model are listed in Eqs. (1–9). In general, the electric field E can be written as:

$$E = -\Delta\varphi - \frac{\partial A}{\partial t} \tag{1}$$

where φ and A are the scalar potential and vector potential.

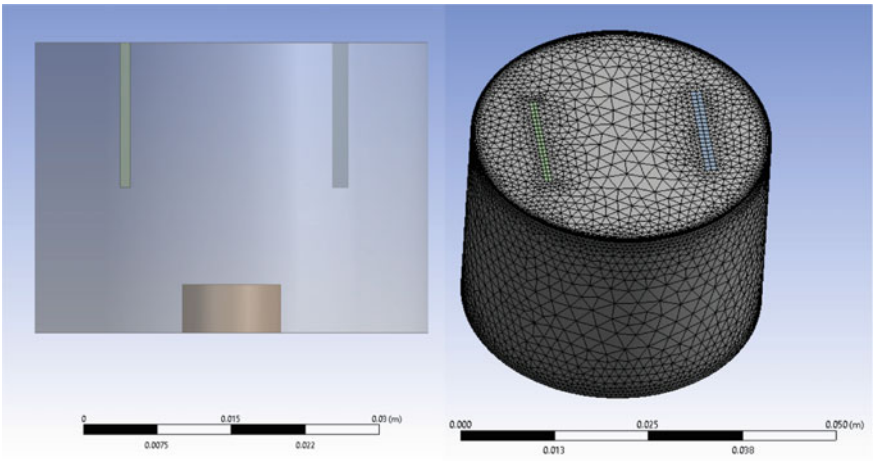

Fig. 1 Model geometry and mesh. (Color figure online)

Table 1 Geometry and mesh data

Geometry data	Mesh data
Cylinder: diameter 4 cm and height 3 cm	Cells: 157,286
Cathode (Cu): 1.5 × 1.5 × 0.1 cm Anode (Al): Al: 1.5 × 1.5 × 0.15 cm	Nodes: 48,943

Ohm's law can be described as:

$$j = \sigma E \tag{2}$$

Here, j = current density, σ = electrical conductivity of media. If U = velocity field and B = magnetic field, it also can be written as:

$$j = \sigma(E + U \times B) \tag{3}$$

As in the steady-state,

$$\frac{\partial A}{\partial t} = 0 \tag{4}$$

Ohm's law can be written as:

$$j = \sigma(-\Delta\varphi + (U \times B)) \tag{5}$$

For sufficiently conducting media, the principle of conservation of electric charge gives:

$$\nabla \cdot j = 0 \tag{6}$$

Therefore,

$$\nabla^2\varphi = \nabla(U \times B) \tag{7}$$

The potential on the boundary can be defined as:

$$\frac{\partial \varphi}{\partial n} = (B \times U)_{\text{boundary}} \cdot n \tag{8}$$

where n = vector normal to the boundary, and

$$\varphi = \varphi_0 \tag{9}$$

φ_0 is a specific potential on the boundary.

Properties of the electrolyte were defined, which is from our previous experimental results [11]. Properties of the anode (Al) and the cathode (Cu) were built-in with the software.

After defining the properties of the electrolyte, thermal and potential conditions and values of those boundaries were set rational and compared to the real experiment. For the final calculation process, we chose solution methods, such as Gauss–Seidel or ILU methods, set reference and initialization values.

Results and Discussion

Current Density Distribution

The vector of the electric current density magnitude is shown in Figs. 2 and 3. In this case we considered, applied Voltage = 1.5 V, distance of electrodes = 2.3 cm, Stirring speed = 12.57 rad/s (120 rpm). Viscosity and electrical conductivity of the electrolyte at 100°C were used. Contact resistance at cathode and anode were both set as 0 ohm-m^2 for the first simulation.

As shown in Figs. 2 and 3, the current density is larger at the bottom and edge of the Cu electrode. That might be one of the reasons for the easy formation of Al dendrite at the bottom and the edge parts of the electrode [11]. Also, the backside of the Cu electrode, which is face to the beaker boundary, has a lower current density than the front side. That is why there is more deposition at the front side than the backside of the electrode in the experiment.

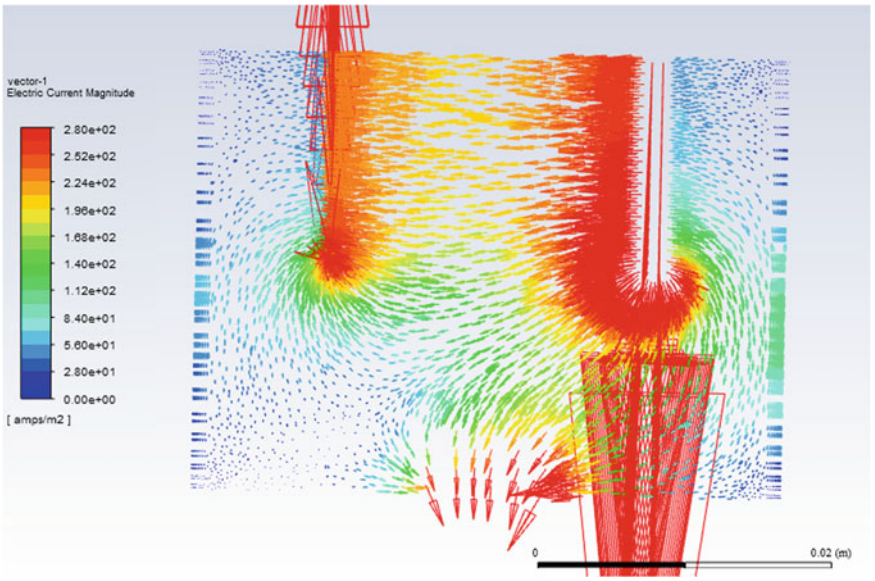

Fig. 2 Distribution of electric current density in the *X*–*Z* plane (left side is Cu cathode and right side is Al anode). (Color figure online)

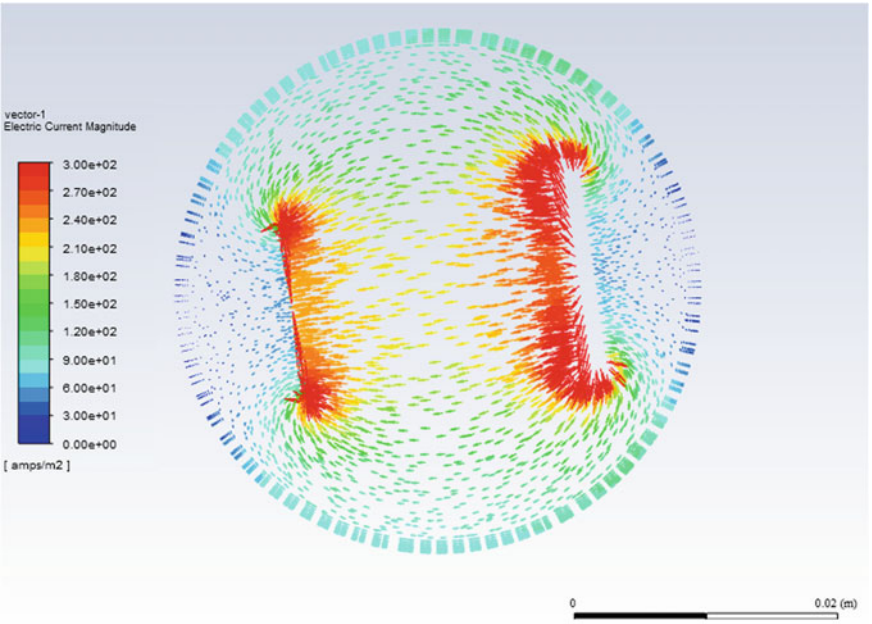

Fig. 3 Distribution of electric current density in the *X*–*Y* plane, 0.005 m from the top of the ionic liquid (left side is Cu cathode and the right side is Al anode). (Color figure online)

Calculation of Secondary Resistances ($R_c + R_{ct}$)

In this modeling approach, we calculated $R_c + R_{ct}$ based on the experimental current density as a function of applied potential, temperature, and surface roughness. In Table 2, the $R_c + R_{ct}$ was given for different applied potential values (Deposition temperature: 100°C; stirring rate: 120 rpm; deposition time: 2 h; surface roughness of Cu electrode: 543.1 ± 59.7 nm; electrode distance: 23 mm; electrolyte BMIC: $AlCl_3$ at a molar ratio of 1: 2).

The relationship between $R_c + R_{ct}$ and the temperature was also simulated. During the simulation, a variation of temperature has changed the conductivity and viscosity

Table 2 $R_c + R_{ct}$ as a function of the applied potential

Applied potential (V)	Experimental current density (A m^{-2}) [12]	$R_c + R_{ct}$ (ohm·m^2)
1	160.1	0.0172
1.25	272.8	0.0138
1.5	357.6	0.0131
1.75	420.6	0.0128

Table 3 Secondary resistances as a function of temperature

Temperature (°C)	Conductivity (S m^{-1}) [our previous work]	Viscosity (kg m^{-1} s^{-1}) [13]	Experimental current density (A m^{-2}) [12]	$R_c + R_{ct}$ (ohm·m^2)
80	2.36	0.0078	167.5	0.023
90	2.73	0.0061	291.3	0.0155
100	3.11	0.00485	396.7	0.012
110	3.34	0.0045	481.7	0.0101

Table 4 $R_c + R_{ct}$ as a function of surface roughness

The arithmetical average surface roughness of Cu cathode: Ra (nm)	Experimental current density (A m^{-2}) [12]	$R_c + R_{ct}$ (ohm·m^2)
543.1 ± 59.7 (320 G)	396.7	0.012
126.7 ± 24.7 (600 G)	419.7	0.0115
78.6 ± 16.4 (800 G)	498.1	0.0101
46.2 ± 8.2 (1200 G)	534.8	0.0095
23.3 ± 4.8 (mirror polishing)	654.6	0.0081

of the ionic liquid. Thus, we set the different conductivities and viscosities of ionic liquid to simulate the secondary resistances at different temperatures.

The variables and results for the study of deposition temperature effect on $R_c + R_{ct}$ are given below (stirring rate: 120 rpm; applied potential 1.5 V; deposition time: 2 h; surface roughness of Cu electrode: 543.1 ± 59.7 nm; electrode distance: 23 mm) (Table 3).

The effect of cathode surface roughness as a function of $R_c + R_{ct}$ is given in Table 4 (deposition temperature: 100 °C; stirring rate: 120 rpm; applied potential 1.5 V; deposition time: 2 h; electrode distance: 23 mm).

In the last part of the study, the effect of electrolyte composition was investigated. The molar ratio of $AlCl_3$ was changed to 1.4, 1.6, 1.8, and 2 where the molar ratio of BMIMCl was fixed to 1. The $R_c + R_{ct}$ decreased with an increasing $AlCl_3$ molar ratio. With the increasing molar ratio of $AlCl_3$, the concentration of $Al_2Cl_7^-$ ion increases [14]. Al_2Cl_7 ion raises the electrical conductivity and reduces the viscosity [15–17]. Because of this, $R_c + R_{ct}$ decreases. The values of secondary resistances are listed in Table 5 (temperature: 100 °C; stirring rate: 120 rpm; applied potential 1.5 V; deposition time: 2 h; surface roughness of Cu electrode: 543.1 ± 59.7 nm; electrode distance: 23 mm).

The correlation between these parameters and surface roughness is given in Fig. 4.

As shown in Fig. 4, the $R_s + R_{ct}$ decreased as applied potential and temperature increased, while increased as surface roughness increased. On the other hand, the redox reaction of Al species is easier to take place at higher potential, temperature, and $AlCl_3$ molar ratio as well as lower surface roughness. So, the contact resistance response to change these variables is expected.

Table 5 $R_c + R_{ct}$ as a function of $AlCl_3$ molar ratio

Molar ratio of $AlCl_3$ (molar ratio of BMIMCl was fixed to 1)	Experimental current density (A m^{-2}) [12]	$R_c + R_{ct}$ (ohm·m^2)
1.4	169.3	0.14
1.6	180.5	0.13
1.8	282.6	0.083
2	396.7	0.057

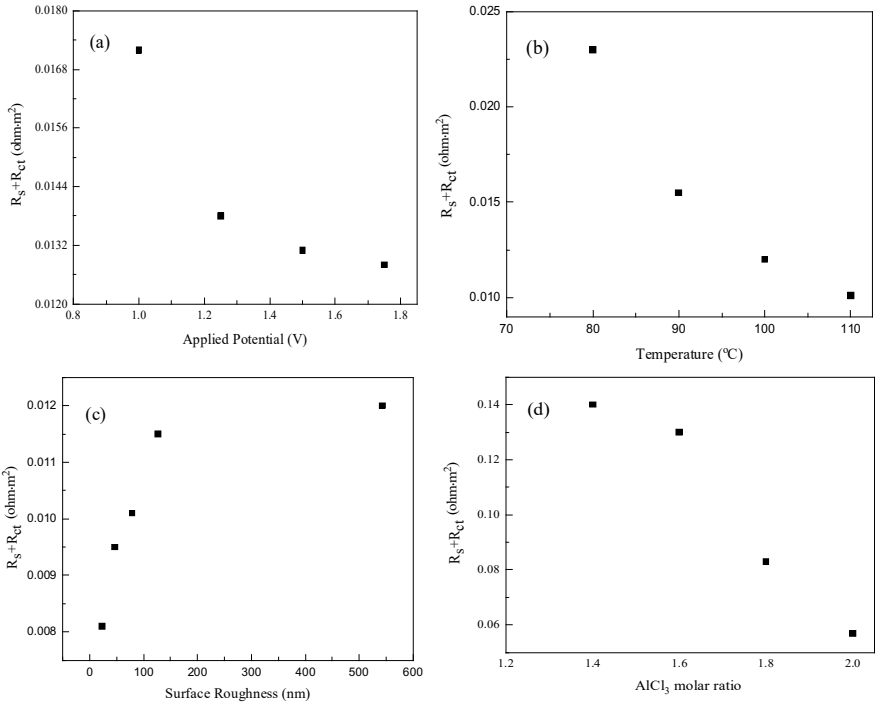

Fig. 4 Variation of secondary resistances in the cell with **a** applied potential, **b** temperature, **c** surface roughness, and **d** $AlCl_3$ molar ratio

Conclusions

A 3-D numerical model of aluminum electrodeposition from chloroaluminate-based electrolyte was developed in ANSYS Fluent. The potential distribution and contact resistance in the electrochemical cell were determined. The result showed that electrode potential is uniform in the electrodes. The contact resistance between the electrode and electrolyte decreased with increasing applied voltage, temperature, and $AlCl_3$ molar ratio. In contrast, increasing surface roughness increased the contact resistance.

Acknowledgements The authors acknowledge the financial support received from the Department of Energy (DOE) RAPID Manufacturing Institute and ACIPCO for this research project. Authors also thank the Department of Metallurgical and Materials Engineering, The University of Alabama for providing experimental and analytical facilities.

References

1. Zhang M, Kamavarum V, Reddy RG (2003) New electrolytes for aluminum production: ionic liquids. JOM 55(11):54–57. https://doi.org/10.1007/s11837-003-0211-y
2. Pradhan D, Reddy RG (2012) Dendrite-free aluminum electrodeposition from $AlCl_3$-1-ethyl-3-methyl-imidazolium chloride ionic liquid electrolytes. Metall Mater Trans B 43(3):519–531. https://doi.org/10.1007/s11663-011-9623-1
3. Zhang M, Kamavaram V, Reddy RG (2005) Aluminum electrowinning in ionic liquids at low temperature. Light Met 2005:583–588
4. Wu B, Reddy RG, Rogers RD (2013) Aluminum reduction via near room temperature electrolysis in ionic liquids. In: Essential readings in light metals, pp 1100–1107. https://doi.org/10.1002/9781118647851.ch161
5. Zhang M, Reddy RG (2017) Modeling of aluminum electrowinning in ionic liquid electrolytes. In: Applications of process engineering principles in materials processing, energy and environmental technologies, pp 65–79. https://doi.org/10.1007/978-3-319-51091-0_6
6. Zhang M, Reddy RG (2006) Ionic liquids electrowinning of aluminum in batch mode cells. Light Met 2006:451–456
7. Popov KI, Djokić SS, Grgur BN (2010) The current distribution in electrochemical cells. In: Fundamental aspects of electrometallurgy. Springer, Boston, pp 101–143
8. Mirzaeian M, Fathinejad H, Mirzaeian M (2015) Effect of the electrode/electrolyte contact resistance on the energy storage capacity and cycleability of Li/O_2 batteries [Abstract]. ECS Meet Abstr. https://doi.org/10.1149/ma2015-03/2/489
9. Wang L, Liu D, Huang T, Geng Z, Yu A (2020) Reducing interfacial resistance of a $Li_{1.5}Al_{0.5}Ge_{1.5}(PO_4)_3$ solid electrolyte/electrode interface by polymer interlayer protection. RSC Adv 10(17):10038–10045. https://doi.org/10.1039/d0ra00829j
10. Mayer S, Geddes LA, Bourland JD, Ogborn L (1992) Faradic resistance of the electrode/electrolyte interface. Med Biol Eng Comput 30(5):538–542. https://doi.org/10.1007/bf02457834
11. Shinde P, Ahmed AN, Nahian MK, Peng Y, Reddy RG (2020) Conductivity of 1-ethyl-3-methylimidazolium chloride (EMIC) and aluminum chloride ($AlCl_3$) ionic liquids at different temperatures and $AlCl_3$ mole fractions. ECS Trans 98:129–139. https://doi.org/10.1149/09810.0129ecst
12. Wang Y (2020) Development of aluminum electrorefining in ionic liquids: the effect of experimental conditions on the deposition behavior and microstructure. MS thesis, The University of Alabama
13. Kamavaram V (2004) Novel electrochemical refining of aluminum based materials in low temperature ionic liquid electrolytes. Ph.D. thesis, The University of Alabama
14. Karpinski ZJ, Osteryoung RA (1984) Determination of equilibrium constants for the tetrachloroaluminate ion dissociation in ambient-temperature ionic liquids. Inorg Chem 23(10):1491–1494. https://doi.org/10.1021/ic00178a039
15. Kim K, Lang C, Kohl PA (2005) The role of additives in the electroreduction of sodium ions in chloroaluminate-based ionic liquids. J Electrochem Soc 152(1):E9–E13. https://doi.org/10.1149/1.1834898
16. Ferrara C, Dall'Asta V, Berbenni V, Quartarone E, Mustarelli P (2017) Physicochemical characterization of $AlCl_3$–1-ethyl-3-methylimidazolium chloride ionic liquid electrolytes for

aluminum rechargeable batteries. J Phys Chem C 121(48):26607–26614. https://doi.org/10.1021/acs.jpcc.7b07562

17. Jiang T, Brym MC, Dubé G, Lasia A, Brisard G (2006) Electrodeposition of aluminium from ionic liquids: part I—electrodeposition and surface morphology of aluminium from aluminium chloride ($AlCl_3$)–1-ethyl-3-methylimidazolium chloride ([EMIm]Cl) ionic liquids. Surf Coat Technol 201(1–2):1–9. https://doi.org/10.1016/j.surfcoat.2005.10.046